AAEC/E475

AAEC/E475

AUSTRALIAN ATOMIC ENERGY COMMISSION

RESEARCH ESTABLISHMENT

LUCAS HEIGHTS

THE APPLICATION OF PROTON INDUCED X-RAY EMISSION TO THE ELEMENT ANALYSIS OF THICK OBSIDIAN SAMPLES

by

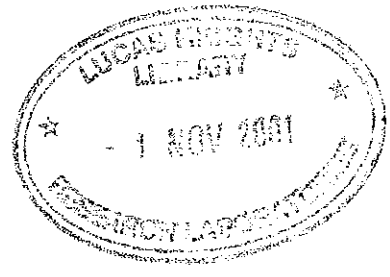

P. DUERDEN
D.D. COHEN*
E. CLAYTON

*Australian Institute of Nuclear Science & Engineering

November 1979

ISBN 0 642 59679 4

AUSTRALIAN ATOMIC ENERGY COMMISSION
RESEARCH ESTABLISHMENT
LUCAS HEIGHTS

THE APPLICATION OF PROTON INDUCED X-RAY EMISSION TO THE ELEMENT ANALYSIS OF THICK OBSIDIAN SAMPLES

by

P. DUERDEN
D.D. COHEN*
E. CLAYTON

ABSTRACT

The proton induced X-ray emission (PIXE) technique has been applied to the analysis of element concentrations in obsidian source samples. No target preparation other than washing and the selection of a flat surface was undertaken. Thick target yields have been calculated and element concentrations derived from the detected X-ray spectra; concentrations are given for K, Ca, Ti, V, Mn, Fe, Ga, As, Rb, Sr, Y, Zr, Nb, Ta and Pb. A pinhole filter is described which enables a single measurement of about 5 minutes' duration to give element concentration data over an X-ray energy range 3-20 keV.

---

*Australian Institute of Nuclear Science & Engineering

Coefficients, Verlag Stahleisen GmbH, Düsseldorf.
Williamson, C.F., Boujot, J. & Picard, J. [1966] - CEA-R3042.
Willis, R.D. & Walter, R.L. [1977] - *Nucl. Instrum. Methods*, 142 : 231-

CONTENTS

1. INTRODUCTION

The analysis of element concentrations in obsidian source material for the classification of artifacts is a major aspect of the archeological study of trade and migration in the obsidian occurring regions of the Mediterranean, the Andean Cordillera, Mesoamerica, Japan and Oceania. The Australian Atomic Energy Commission (AAEC) is participating in an investigation of obsidians from the latter region, particular interest being centred on the South West Pacific. A review of characteristic and geographic distributions of volcanic glasses in Oceania has been made by Smith *et al.* [1977]. Source samples are available from all known flows in the region, the majority of them being from New Britain, the d'Entrecasteaux Group, the New Hebrides and New Zealand. Samples are also available from Easter Island, Hawaii, Indonesia and Australia.

The classification of element concentrations in obsidian samples has been reported by many researchers and several analysis techniques have been used, including emission spectroscopy, neutron activation and X-ray fluorescence. Nielson *et al.* [1976] reported the element analysis of obsidian artifacts by proton induced X-ray emission (PIXE). Using thin targets made from acid digests of 30 to 100 μg of finely powdered samples, they reported concentrations of the elements K, Ca, Ti, Ba, Mn, Fe, Zn, Ga, Rb, Sr and Zr.

The PIXE technique has been used at the AAEC's Research Establishment at Lucas Heights to analyse thick obsidian targets which generally were either chips or cut samples of volcanic flows and artifacts in their entirety. No target preparation, apart from washing and selection of a flat surface, was necessary. The source samples were easily distinguished both by element concentration from the complete X-ray spectrum and by a much simpler intercomparison of counts in specific channels set by X-ray energy windows.

The experimental assembly at Lucas Heights is described in detail. A pinhole filter which may be used for data collection in the entire 1.5 to 40 keV region, but having the facility for high count acquisition in the lower and higher energy regions, is discussed.

Data analysis procedures for both element concentration measurement and for the intercomparison of spectra have been established and are described in full. The calculation of K X-ray and L X-ray yields for elements in a thick obsidian matrix is described and yield curves are

obtained. Possible errors that can arise from rough surfaces and incorrectly positioned targets are included in the discussion.

Data from about 40 source samples have been used in this study; a number of source regions within the New Britain area are included. Approximately 20 elements can be resolved and are used for source intercomparison. Most of the analysed data have been converted to element concentrations. Element concentrations are given for K, Ca, Ti, V, Mn, Fe, Ga, Rb, Sr, Y, Zr, Nb, Ta and Pb; important elements for the obsidian classification are mentioned and some variations in these analyses are highlighted. Silicon data are used in the relative element concentration analysis, but are not included in the list of element concentrations. The detector efficiency is not well determined at the Si K X-ray energy (1.74 keV) and changes very rapidly with energy, nor is the detected silicon X-ray yield certain as it is very dependent on the unknown concentration of lighter Z elements in the particular obsidians. Copper and zinc appear to be useful elements for the analysis, but in this particular experiment there has been some Zn and Cu contamination from the target holder.

2. EXPERIMENTAL PROCEDURES

The standard PIXE experiments undertaken at the AAEC Research Establishment have been fully described by Cohen & Duerden [1979]; a schematic diagram of the equipment is shown in Figure 1.

A 2.26 or 2.5 MeV proton beam is used to irradiate targets loaded on a 1 m long target holder, the position of which can be varied by a computer-controlled stepping motor. X-rays emitted by the target material are detected by an intrinsic silicon detector placed beneath the target chamber; there is a 25 μm Be window in the base of this chamber. Two thin layers of Perspex, one having a pinhole at the centre, are used as filters and may be placed in the path of the X-rays between the target chamber and the detectors. The target chamber is insulated ($\gtrsim$ 70 MΩ) from the rest of the experiment and acts as a Faraday cup for charge collection and integration to give a measure of the total current hitting the target.

The obsidian samples vary in size from small chips to pieces ~ 50 mm in diameter with thicknesses ranging up to 20 mm. The only limitations are the size and shape of the samples; they must be able to be mounted on the target holder and, if the target is to be moved, able to go into

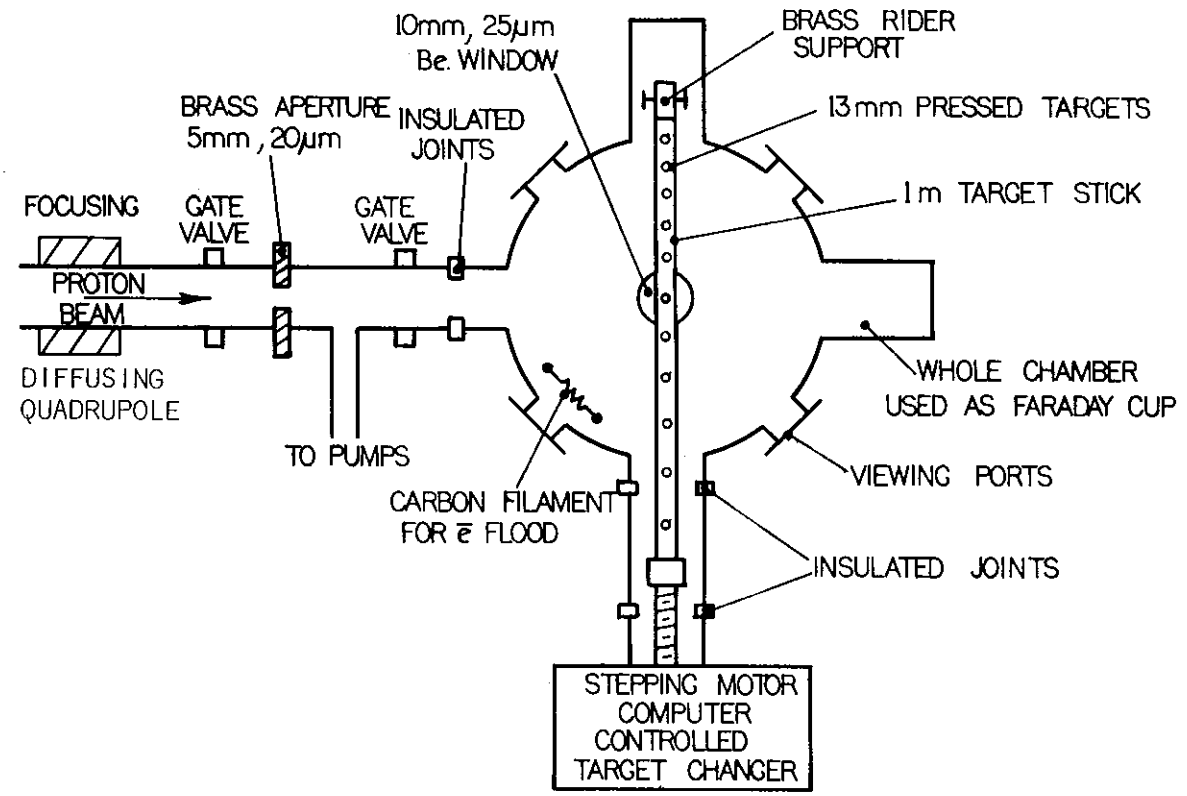

PIXE CHAMBER TOP VIEW

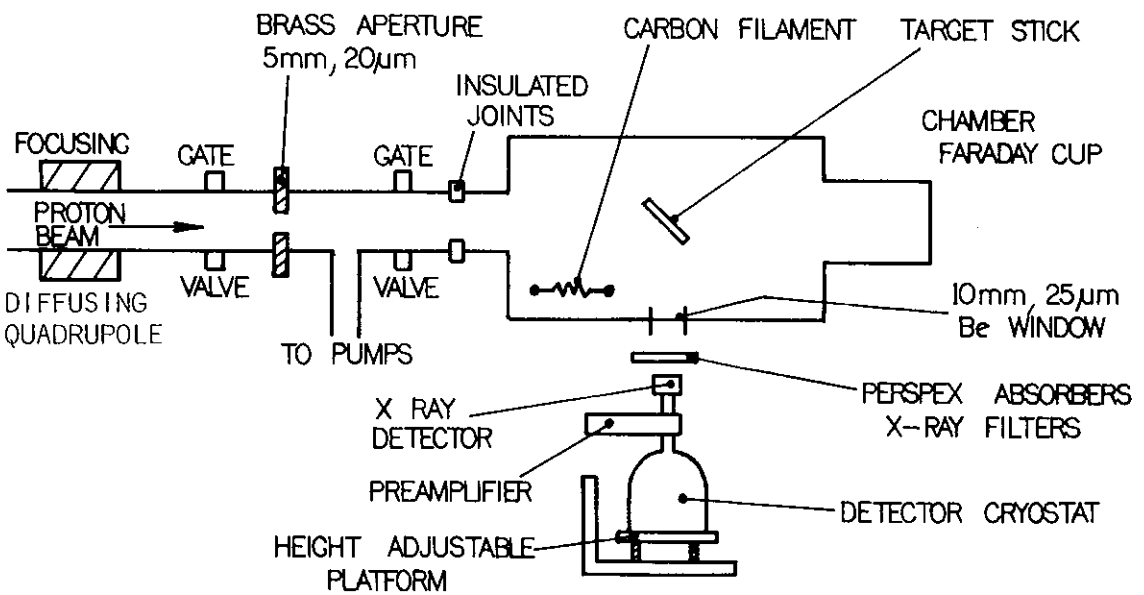

PIXE CHAMBER SIDE VIEW

FIGURE 1. SCHEMATIC DIAGRAM OF THE EQUIPMENT

the 50 mm diameter side tube. The samples are positioned such that an approximately flat surface is presented to the beam at an angle of 45° to both the incoming proton beam and the emitted X-rays.

The sources for the present experiment are itemised in Table 1. The only target preparation was to wash the samples in distilled water and Mallinckrodt Nanograde benzene using ultrasonic agitation. The majority of samples irradiated in the preliminary run had smooth, cleaved surfaces but a number had flat ground surfaces. The effect of variation in target angle and of the errors resulting from misplacement of the target will be discussed later.

A carbon filament for flooding the insulated targets with electrons is attached to the top of the chamber which is kept at a base pressure of approximately 0.5 mPa.

A complete description of the electronic equipment (Figure 2) is given by Cohen & Duerden [1979]. The detector is an intrinsic hyper-pure n type silicon chip and has an active area of 50 cm and a depletion depth of 5 mm. The resolution (FWHM) was measured to be 285 eV for the Mn Kα 5.9 keV X-ray; this rises to 325 eV for the Zr Kα 15.77 keV X-ray.

2.1 Detector Efficiency

Measurements of the detector efficiency with varying numbers of layers, T, of 1.5 mm Perspex inserted between the chamber and the detector have been reported by Cohen & Duerden [1979]. The efficiency of the detector, Eff %, at an X-ray energy, E, takes the form:

$$\text{Eff \%} = 100 \exp[-588\ T/E^3] \quad . \quad 6 < E < 20 \text{ keV} \qquad (1)$$

The efficiency of the detector when there is no filter in place can be represented by:

$$\text{Eff \%} = 100 \exp[19.93\ E^{-2.835}] \quad . \quad 1.6 < E < 20 \text{ keV} \qquad (2)$$

This takes into account the two 25 μm beryllium windows and the 3 cm air gap that are interposed between the detector and the target, and the 50 $\mu g\ cm^{-2}$ of gold that is present on the crystal surface. The detector efficiency is shown in Figure 3 for the no filter and the 3 mm Perspex filter cases.

2.2 Measurements

A typical spectrum obtained when no filter is in place is shown in Figure 4. Good data are obtained for the elements Si, Cl, K, Ca, Ti, Mn, Fe, Cu and Zn. The maximum data acquisition rate of 3000 counts per

TABLE 1

OBSIDIAN SOURCE SAMPLES USED IN PRESENT EXPERIMENT

Ident. No.	Region	
SE.SZ.34.A12 SE.SZ.34.A9 SE.SZ.34.A8	Santa Cruz	Solomon Islands
	Tikopia	
175	Dire	New Britain
287/A	Mt Bao	
187	Talasea	
295	Hospital	
292	Bitokara	
296/1	Bitokara	
292/1A	Bitokara	
298	Admin	
299A	Garua	
293/2	Voganakai	
293/1A	Voganakai	
294	Pilu	
180/1	Waisisi	
304/4	Iaupolo	West Fergusson
392/2	Igwageta	
250	Gaua	New Hebrides
316/2C	Gaua	
250A	Gaua	
249A	Vanua Lava	
249	Vanua Lava	
280	Lou Island	Admiralty
283/A	Pam	
283/1	Pam	
277A	Lakou	
281A	Umrei	
1974/29	Te Mamavai	Easter Island
17691E	Maunga Orito	
	Hala'uta	Tonga
	Tefitomaka	
GW373	Weta	New Zealand
GS628	Cook's Bay	
132/49B	Pitcairn	
P40908A	Kermadecs	
352/H	Puu Waawaa	Hawaii
301/A	Dobu	East Fergusson

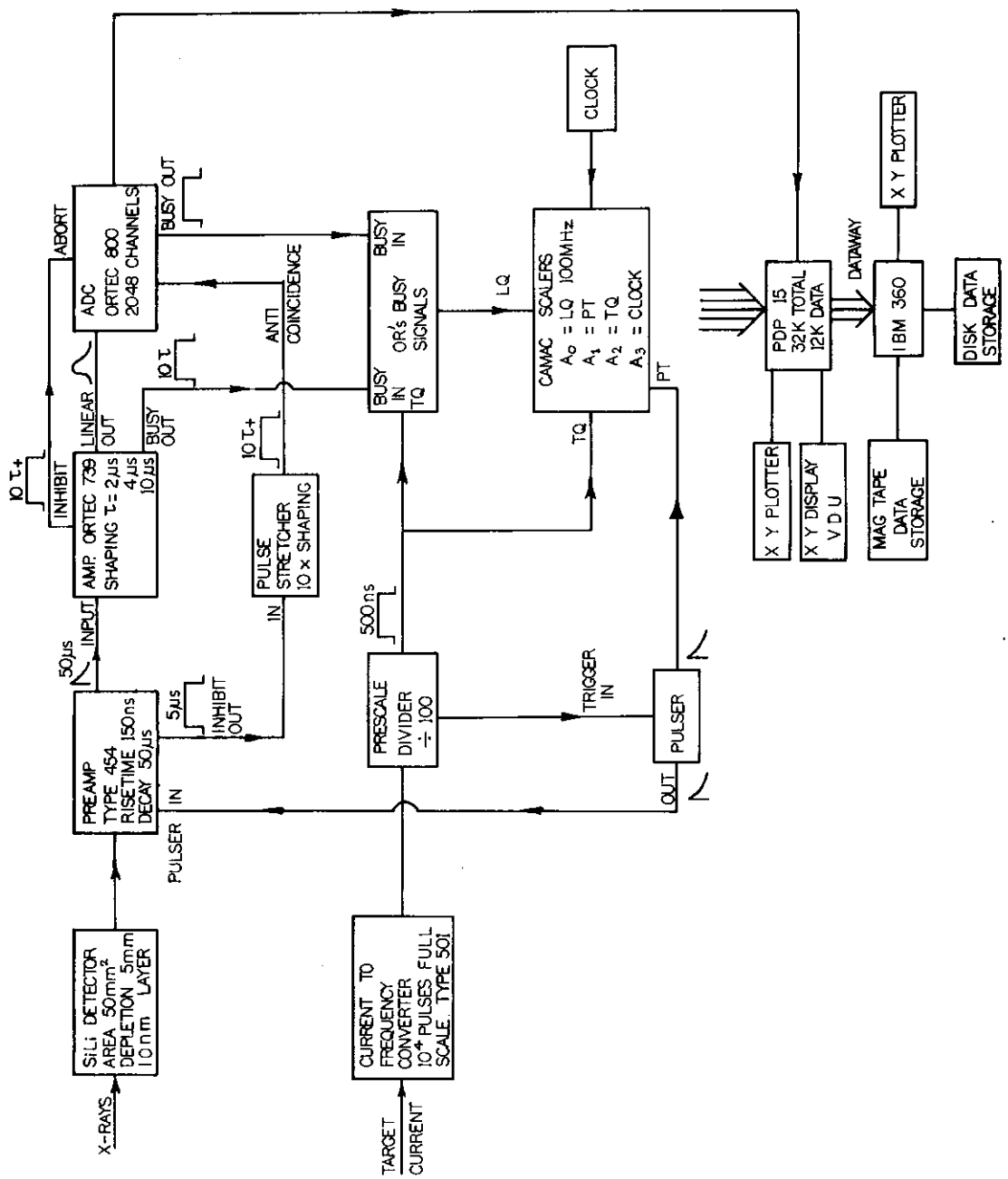

FIGURE 2. SCHEMATIC DIAGRAM OF THE ELECTRONICS SYSTEM

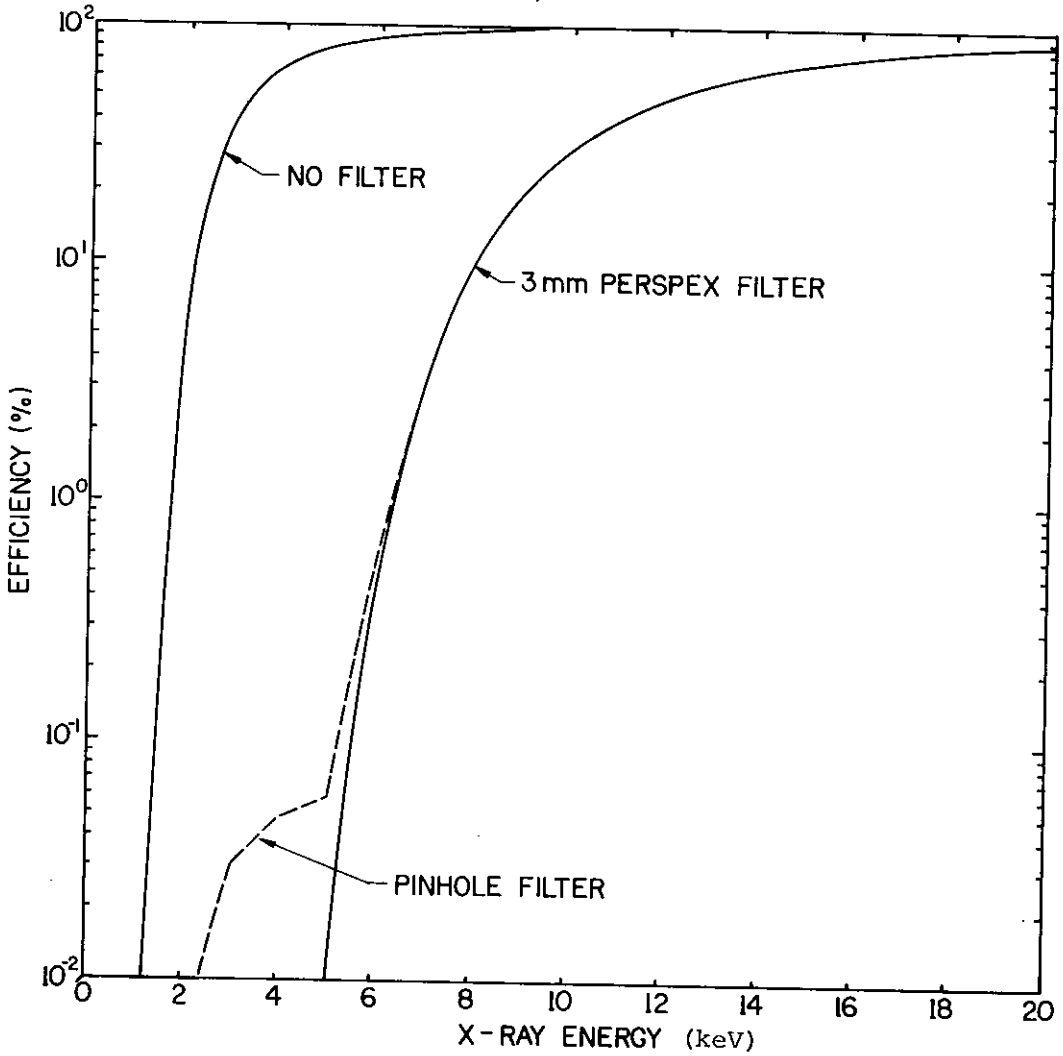

FIGURE 3. EFFECT OF FILTER ON DETECTOR EFFICIENCY

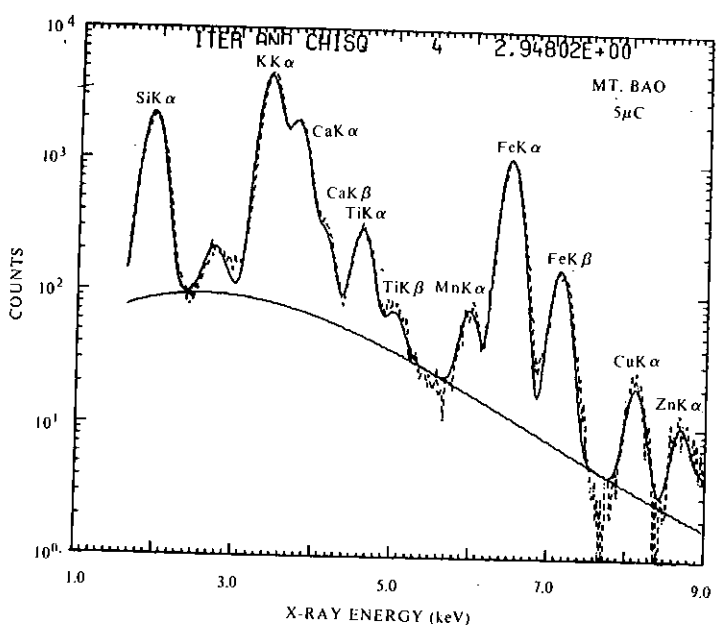

FIGURE 4. OBSIDIUM SPECTRUM - NO FILTER

second is reached with a current of ~ 20 nA and an aperture allowing only one sixteenth of the detector area to be used. A typical run of 5 μC live charge lasted approximately four minutes.

The use of the 3 mm Perspex layer absorbs the low energy X-ray continuum and the bulk of the characteristic X-rays of the obsidian samples (from Si, K, Ca and Fe) and reduces the data acquisition rate to 1/10 000 of the no filter case. The full detector area can now be used and the target current increased to ~ 200 nA, and yet the data acquisition rate will still only be ~ 200 to 300 counts per second. A typical spectrum obtained with the filter is shown in Figure 5. Good data can be obtained for the elements Fe, Ni, Cu, Zn, Ga, As, Rb, Sr, Y, Zr, Nb, Ta and Pb. Typical runs were of 40 μC live charge and lasted approximately five minutes.

It is obviously desirable that a single filter be devised so that the complete element data can be obtained in a single experiment. To achieve this the total diameter of the detector (8 mm) has been covered with a 3 mm Perspex pinhole filter having a central hole, the size of which is selected to enable the lower energy spectrum peaks (particularly the Si, K, Ca and Fe Kα peaks) to be attenuated to approximately equal the peak areas from high energy Rb, Sr and Zr Kα X-rays. The problem of sum peaks is removed because the count rate into any peak within the detector spectrum is very low. The maximum target current that can be used on the sample under analysis determines the limitation to the data acquisition rate. In our analysis, the maximum target current was 200 nA and the pinhole size was 0.21 mm diameter, *i.e.* 1/1450 of the full diameter. When using this filter, the efficiency is

$$\text{Eff } \% = 100[\exp(-588 \times 2/E^{-3}) + \frac{1}{1450}\exp(19.93\ E^{-2\cdot835})] \quad 1.6 < E < 20 \text{ keV} \qquad (3)$$

and is included in Figure 3. The effect of the filter is seen in Figure 6. Runs were of 40 μC live charge and lasted approximately five minutes. Care is needed in such experiments to see that there is good alignment between the filter pinhole, the target area and the detector.

All samples were analysed with and without the 3 mm Perspex filter and a number were analysed with the pinhole filter to enable these data to be compared with more simply analysed data.

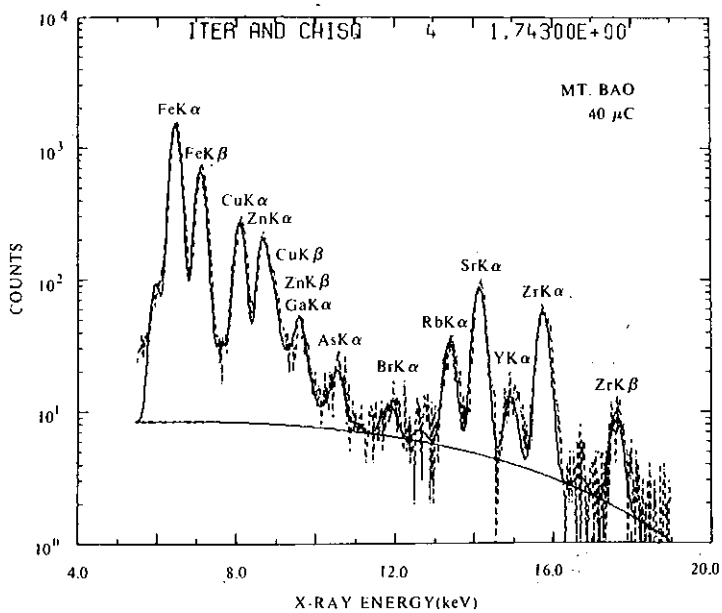

FIGURE 5. OBSIDIAN SPECTRUM - FILTER 3mm PERSPEX

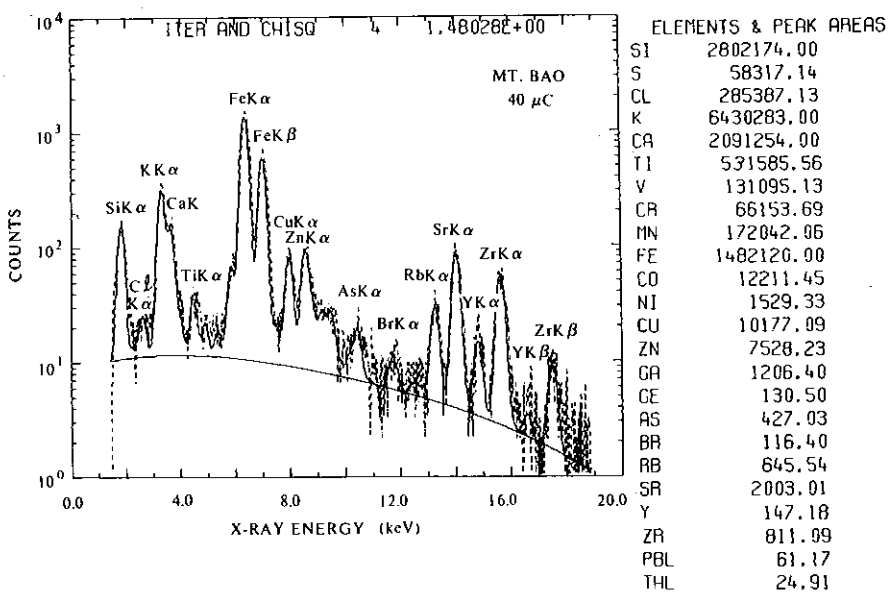

FIGURE 6. OBSIDIAN SPECTRUM - PINHOLE FILTER

3. DATA ANALYSIS

The analytical routines and computer programs used for the analysis is fully described elsewhere [E. Clayton - AAEC report in preparation].

The characteristic X-ray peaks are assumed to be superimposed on a smoothly varying background which is fitted by a five parameter exponential of the form:

$$b_i = \exp[P_0+P_1E_i + P_2E_i^2 + P_3E_i^3 + P_4E_i^4] \quad . \tag{4}$$

The X-ray peaks are represented by Gaussian line shapes. Large peaks, however, are seen to be asymmetric, hence low energy tails and step functions can be included in the analysis. The analytical data are fitted, channel by channel, to a function of the form:

$$Y_i = b_i + \Sigma_{jk} A_j \Sigma R_{jk} G_{ijk} \ , \tag{5}$$

where R_{jk} is a matrix of the relative peak intensity of X-rays at energies E_{jk} for element j; A_j is the magnitude of the Kα or Lα peak, and G_{ijk} the Gaussian peak shape

$$\exp\left[\frac{(E_i-\mu)^2}{2\sigma^2}\right] \ ,$$

where $\mu = P_5 + P_6E_{jk}$; and $\sigma = P_7 + P_8E_{jk}$. The Gaussian peak shape is is modified by a tail function:

$$T = P_9 \exp P_{10}(E_i-\mu) \quad E_i < \mu \tag{6}$$

and a step function

$$S = P_{11} \operatorname{erfc}\left[\frac{(E_i-\mu)}{\sigma\sqrt{2}}\right] \quad . \tag{7}$$

The parameters P_5 to P_{11}, together with A_j and the complete background continuum b_i, were varied in a least squares fitting program until χ^2, defined by Equation (8), changed by less than 1 per cent:

$$\chi^2 = \frac{1}{N-P} \sum_i \frac{(Y_i-Y_{expt})^2}{\sigma^2_{expt}} \ , \tag{8}$$

where P is the number of parameters; N is the number of channels used for fitting; and Y_i, Y_{expt} are fitted and experimental yields, respectively, for channel i and have a standard deviation σ_{expt}.

The relative peak intensity data, R_{jk}, for the element j included in the analysis code, is applicable for X-ray detection when there is no

filter material of any kind between the detector and the target. The attenuation data for the varying thicknesses of Perspex filters are also included in the analysis program which adjusts the R_{jk} data for the particular filter case. The peak areas associated with the Kα or Lα X-ray lines of the particular element are then extracted and, if necessary, the peak areas obtained in a filter case can be normalised to the zero filter efficiency condition.

The zero filter data were analysed over the energy range 1.6 to 9 keV. The two Perspex filter data were analysed over a range 6 to 19 keV and all peak areas were brought up to the zero filter condition. The pinhole filter data were analysed from 1.6 to 19 keV and again brought to the zero filter efficiency. Examples of the fitting analyses are shown in Figures 4, 5 and 6; the smoothly varying background and the Gaussian line shapes can be seen fitted to the experimental data.

4. YIELDS

The X-ray yield from trace elements in a 'thick' target has been calculated by the method described by Cohen *et al.* [1979]. They considered the two major problems resulting in reduced X-ray yield - that proton energy loss is due to collisions with matrix atoms and that X-rays produced at varying depths in the matrix are attenuated while traversing the matrix en route to the detector.

Following the prescription of Willis & Walter [1977] for the total thick target K or L X-ray yield, we have:

$$N^{K,L} = \left[\frac{CN_o}{W}\right]\left[\frac{\Omega It\varepsilon}{4\pi e}\right]\int_{E_p}^{o} \sigma_x^{K,L}\,\frac{dE}{S(E)}\,\exp\left[-\mu\int_{E_p}^{E}\frac{dE}{S(E)}\,\cot\theta\right] \qquad (9)$$

where $\sigma_x^{K,L}$ = $\sigma_I\bar{\omega}_{K,L}$ is the X-ray production cross section for all K or L transitions (cm^2);

μ = $\Sigma\mu_j c_j$ is the composite matrix mass attenuation coefficient (cm^2 g^{-1});

$S(E)$ = $\Sigma S_j c_j$ is the composite proton stopping powers of the matrix (MeV cm^2 g^{-1});

σ_I = the proton ionisation production cross section for the trace element being considered;

$\bar{\omega}_{K,L}$ = the mean fluorescence yield for all K and L transitions;

μ_j = mass attenuation coefficient of the j^{th} matrix element;
S_j = proton stopping power of the j^{th} matrix element;
c_j = the relative concentration by weight of the j^{th} matrix element;
C = the relative concentration by weight of the trace element;
N_o = Avogadro's number;
W = the atomic weight of the trace element (g);
Ω = the solid angle subtended by the detector (sr);
It = the total proton charge impinging on the target (C);
ε = the detector efficiency including all absorptive materials between the detector and the target;
$\equiv$ Eff % as defined by Equation (1) in our case;
e = electronic charge (C);
E_p = initial proton energy (2.26 or 2.5 MeV); and
θ = target angle (45°).

The mass attenuation coefficients and stopping powers required to produce these curves were taken from the tables of Theisen & Vollath [1967] and Williamson *et al.* [1966], respectively, and the ionisation production cross sections were calculated by the polynomial fit of Johansson & Johansson [1976] and the fluorescence yields from the tables of Bambynek *et al.* [1972]. As far as can be estimated, these would produce a possible error in the total X-ray count of between 5 and 15 per cent.

A calculation of the thick target yield from a US National Standards Bureau geological standard rock (BCR-1) has been compared with experimental measurements of a pressed capsule of the ore sample. The results are shown in Figure 7. The shape of the yield curve is in good agreement with the experimental data for all elements with $Z > 19$, but an overall normalisation factor has to be applied to the yield data.

Similar results have been reported by Liebert *et al.* [1973] who have measured a detector efficiency that is 13 per cent lower than that stated by the manufacturer. They attributed this to a geometrical factor correcting for losses due to apertures or annular dead areas inside the detector case. In the present experiments the need for normalisation could, however, be partially due to a systematic error in our measurement of the total charge hitting the target.

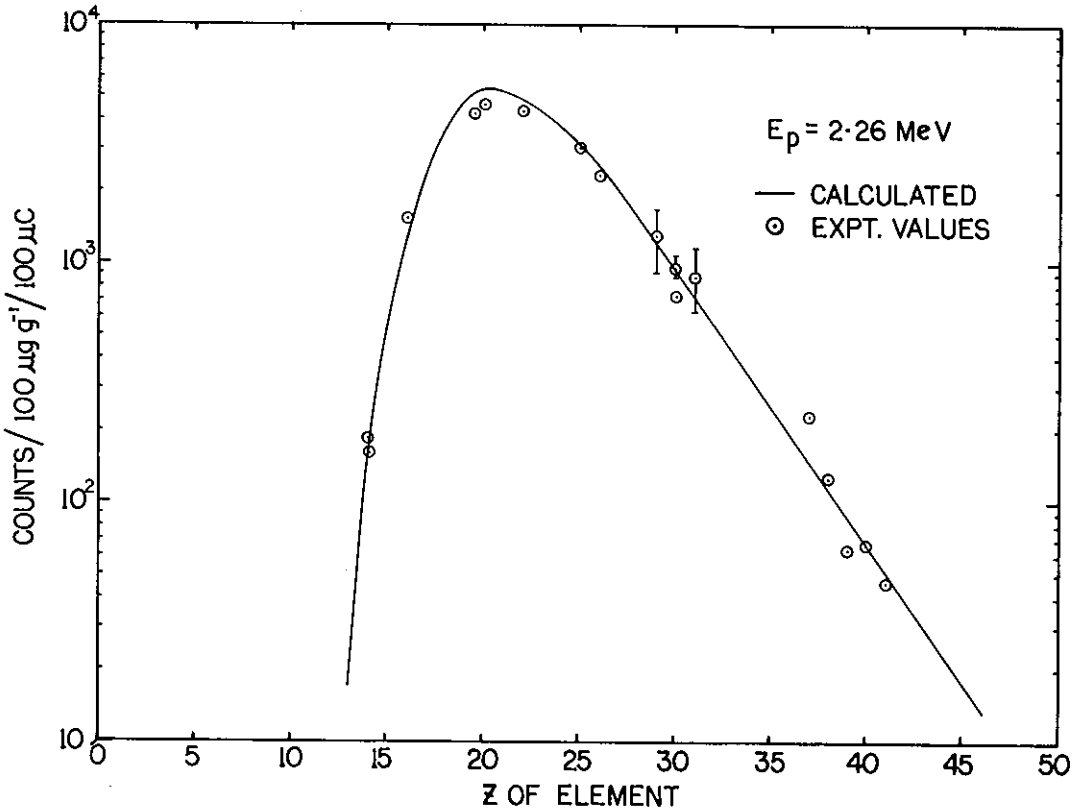

FIGURE 7. CALCULATED AND MEASURED X-RAY YIELD FOR THE STANDARD BCR-1

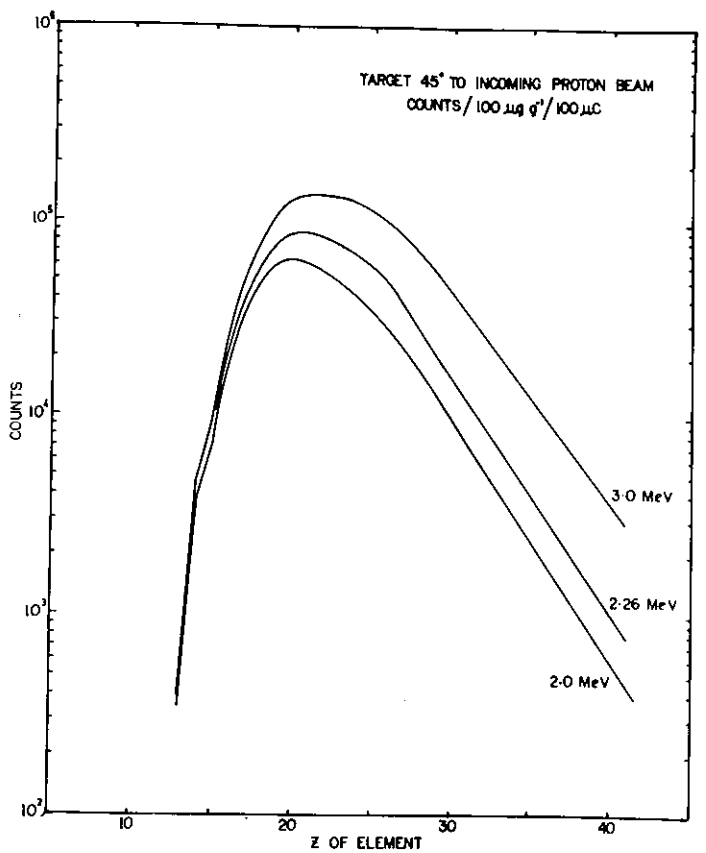

FIGURE 8. VARIATIONS OF K_α X-RAY YIELD WITH ENERGY

A similar calculation has been used for X-ray yields from a thick obsidian matrix. The concentrations of the major elements in this matrix were taken from X-ray fluorescence analyses carried out at Macquarie University and at the Australian National University's Geology Department, reported by Ambrose [1976] and included in Table 2. The derived element concentrations for the Santa Cruz (Solomon Islands) obsidians (see below) suggests that the concentration of major elements in these samples may be different from those in other samples. A larger uncertainty in the calculation of the X-ray yield using the Ambrose data will apply for these samples.

Comparison of some of the measured data with published element concentrations for some of the obsidian samples gave the normalisation factor for this particular experiment.

TABLE 2

MAJOR ELEMENT CONCENTRATIONS IN TYPICAL OBSIDIAN SAMPLES

Element	Conc. %
Si	35
O	50
Al	7
Fe	1
Na	3
Ca	1
K	3

The number of Kα X-rays detected at the 50 mm^2 crystal/100 μC/100 μg g^{-1} for a proton beam of 2.0, 2.26 and 3.0 MeV at 45° to the target and to the detector is shown in Figure 8. The variation in yield as a function of outgoing angle is shown in Figure 9 for a 2.26 MeV proton beam where the yield for a particular Z is normalised to the value $\Sigma(Y55° + Y45° + Y35°)/3$.

It can be seen that large changes in the estimation of the element concentration can occur for low Z elements with quite small alteration in target angle. This has been verified experimentally and the experimental measurements are included in Figure 9. For source identification, the ratio of yields for adjacent or similar (Z) elements will be valuable

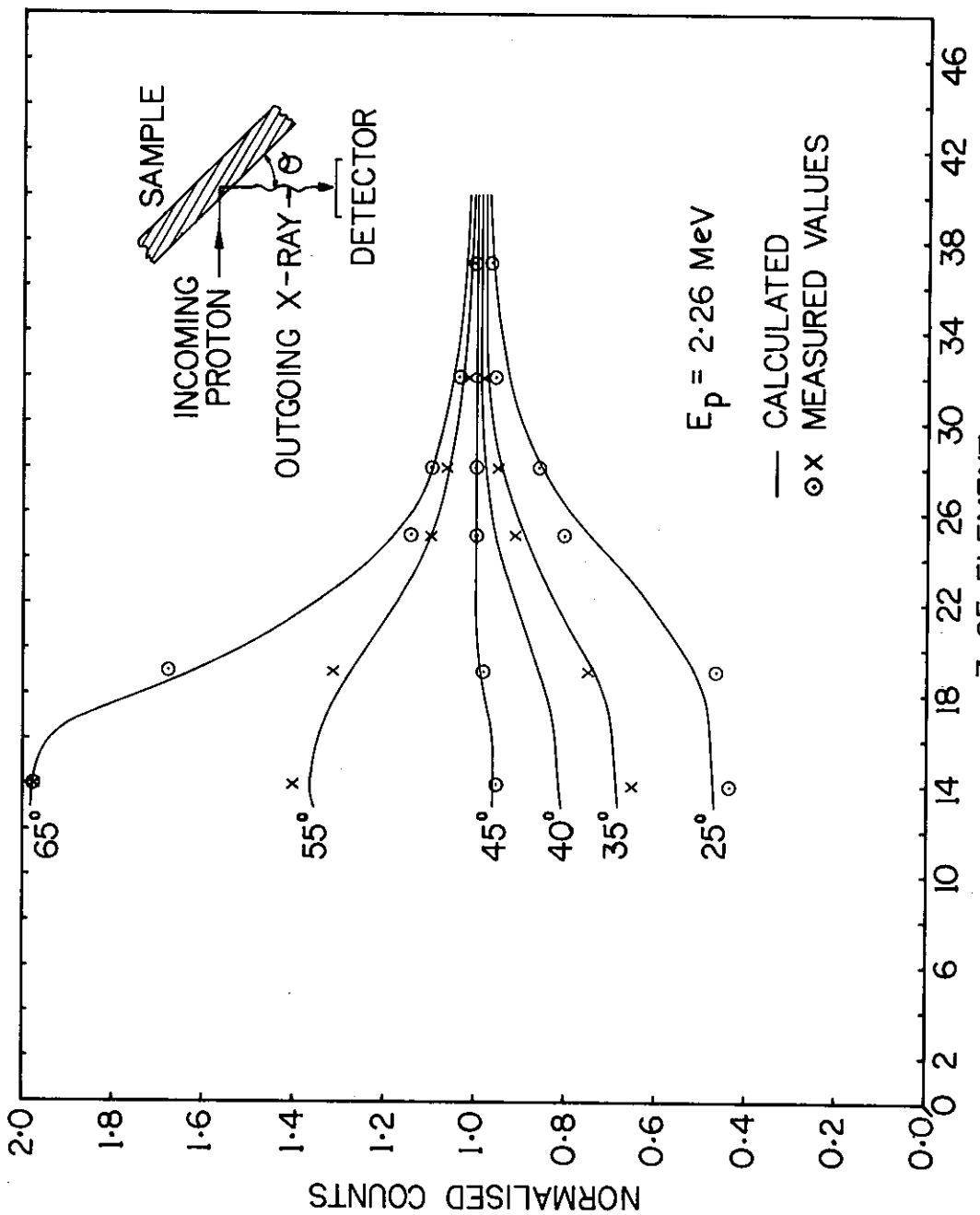

FIGURE 9. VARIATION OF DETECTED X-RAY COUNTS WITH CHANGE IN INCIDENT ANGLE OF PROTON BEAM

and will be much less sensitive to any change in target angle. In this experiment, a variation in angle of ± 5° was considered possible; this would give a variation in the yield for Si of ± 12 per cent. The Si/K ratio would, however, vary by only ± 2 per cent.

Small changes in the proton energy during an analysis can give rise to variation in the X-ray yield. From Figure 8, it can be seen that this variation in yield is between 0.2 per cent and 0.6 per cent for 1 per cent change in proton energy over the range of elements being considered. There will, therefore, be no significant errors in any ratio of element yields resulting from drift in the proton energy which is stabilised to $\leqslant$ 0.5 per cent. The Kα X-ray detected yields for 2.26 and 2.5 MeV are given in Table 3.

TABLE 3

Kα X-RAYS DETECTED/100 μC/100 μg g^{-1}

Element	2.26 MeV	2.5 MeV	Element	2.26 MeV	2.5 MeV
Si	3535	3713	Ga	11740	17480
K	70690	82965	As	6776	10217
Ca	81943	99253	Rb	2276	3529
Ti	69604	88746	Sr	1743	2718
V	62674	82096	Y	1343	2120
Mn	46822	64156	Zr	1035	1634
Fe	39595	55239	Nb	798	1260
Ni	25895	37129	Ta (L)	11742	16941
Cu	19698	28590	Pb (L)	4112	6170
Zn	15454	22673	Th (L)	1550	2395

No Perspex filter used.

$\Omega = 2.2 \times 10^{-3}$ *Sr*

5. SECONDARY Kα X-RAY PRODUCTION

The enhancement of the X-ray production of an element A by excitation from the radiation of an element B within the obsidian matrix has been considered using the calculational procedure outlined by Reuter *et al.* [1975]. They showed that the secondary fraction caused by element B, of the total primary Kα product for element A, where $Z_B > A_A$, is:

$$\frac{Y_{sec,A}}{Y_{PRIM,A}} = \frac{1}{2}\left(\frac{r_A-1}{r_A}\right) C_B \frac{A_A}{A_B} \frac{\sigma_{K\alpha,B}}{\sigma_{K\alpha,A}} \frac{\mu_{K\alpha,B}(\text{in A})}{\mu_{K\alpha,B}(\text{in obsidian})} \cdot \omega_{KB} \quad (10)$$

where C_B is the concentration by weight of B in the obsidian;

$\mu_{K\alpha,B}$ in A is the mass absorption coefficient for a Kα X-ray of element B in matrix A;

$\mu_{K\alpha,B}$ in obsidian is the mass absorption coefficient for a Kα X-ray of element B in the obsidian matrix;

A_A is the atomic weight of A;

A_B is the atomic weight of B;

ω_{KB} is the K fluorescence yield of element B;

$\sigma_{K\alpha,B}$ is the Kα X-ray production X section for element B; and

r_A is the K absorption edge jump ratio.

Reed [1965] gives a value of 0.88 for the $\frac{r_A-1}{r_A}$ ratio.

The maximum contribution of secondary X-ray production was found in the Santa Cruz (Solomon Islands) samples and contributed only ~ 1 to 2 per cent to the total X-ray yield of the Mn Kα X-rays. The contribution of the effect has not been considered in subsequent analysis.

6. RESULTS

The normalisation factor of 0.80 ± 0.07 for the element concentration calculation was found by comparison of peak area/X-ray yield data with published element concentrations. The standard error has been obtained from nine element ratios and the sources of the data used in the comparison is shown in Table 4.

The element concentrations obtained with the peak areas, the calculated X-ray yields and the derived normalisation factor are listed in Table 5; the standard errors quoted for each element have been obtained by adding the normalisation error and the statistical error. Table 6 lists some important interelement concentration ratios and includes a Si/K peak areas ratio.

It can be seen that a wide range of concentrations can be measured in the same experiment with a detector resolution of 285 eV at the Mn Kα X-ray, provided that a good analytical program is available for resolving overlapping Kα/Kβ X-rays.

TABLE 4

SOURCES OF COMPARABLE DATA

Sample	Elements	Reference
Maunga Orito Hawaii Vanua Lava Garua	Rb, Sr, Y, Zr	Smith *et al.* [1977]
East Fergusson (Younger) Dobu St Andrew Strait	Fe, Rb, Sr, Y, Zr	Smith [1974]
Talasea	K, Ca, Ti, Mn, Fe, Sr, Zr	Key [1969]
Pam Waisisi West Fergusson	K, Ca, Mn, Fe, Rb, Sr, Y, Zr	Ambrose [1976]
Tefito Tonga	Mn, Rb, Sr, Zr	Rogers [1974]
Cook's Bay Weta	Ti, Mn, Rb, Sr, Zr	Reeves & Ward [1976]

A large number of samples have been analysed, and we expect to publish much of the data. It was observed that measurements on different samples from the same source region, whether of cut, cleaved or with rough surfaces, gave consistent values of the element ratios, and comparisons of measured concentrations made on different samples of the group over several months gave experimental variations of ~ 7 per cent. Examination of repeated measurements of interelement ratios showed that the ratios agreed within the statistical accuracy of the counts in the peak areas.

The majority of the source samples are separable either by direct examination of the element concentrations or by comparison of the interelement ratios. The variations in the measured concentrations of K, Ca, Ti, Fe, Sr, Rb and Zr are seen to be particularly significant for source identification. However, concentrations of some other elements appear to be good indicators for particular samples. Yttrium concentrations are high for the Easter Island samples; a high concentration of arsenic is measured in the Weta sample and high concentrations of gallium are seen in the Easter Island and Pitcairn Island samples; niobium and vanadium are not detected for a number of the samples. The very high concentrations of niobium and tantalum in the Santa Cruz samples are

TABLE 5

COMPOSITION OF OBSIDIAN SAMPLES USING PIXE TECHNIQUE

Element		K	Ca	Ti	V	Mn	Fe	Ni	Ga	As	Rb	Sr	Y	Zr	Nb	Pb	Th	Ta
		%			μg g^{-1}		%	μg g^{-1}										%
Standard Error on Element Concentration		± 9%	± 9%	± 10%	± 13%	± 11%	± 9%	± 9%	± 9%	± 9%	± 9%	± 9%	± 9%	± 9%	± 9%	± 9%	± 9%	± 9%
A12	Solomon Islands	0.96	5.39	3.67	1070	9500	11.2	460	560	170	62	270	3120	6950	11500	-	465	1.19
A9		1.11	9.06	4.11	930	7740	11.5	390	500	150	32	450	2430	5690	9420	-	350	1.09
A8		0.53	3.99	2.45	490	4880	4.91	290	370	115	44	230	1170	3700	7710	-	217	0.66
Tikopia		1.15	6.10	0.35	-	2220	5.15	54	45	120	65	215	34	305	23	9	-	-
Dire	New Britain	2.51	0.70	0.14	84	460	0.885	77	24	18	65	245	20	158	-	18	-	-
Mt Bao		2.34	0.66	0.13	-	410	0.855	24	20	15	61	228	11	157	-	2	-	-
Talasea		2.89	0.81	0.14	44	420	0.920	65	23	15	61	228	11	138	-	4	-	-
Hospital		2.80	0.78	0.14	120	455	0.905	55	17	13	54	226	22	136	-	10	-	-
Bitokara		1.85	0.53	0.12	39	350	0.855	28	21	12	61	225	12	141	-	5	-	-
Admin		*	*	*	*	*	0.830	71	16	15	61	235	16	149	-	11	-	-
Garua		1.95	0.42	0.093	-	355	0.585	44	18	12	65	147	10	141	-	10	-	-
Voganakai		2.50	0.59	0.13	120	325	0.870	39	18	13	66	176	13	149	-	5	-	-
Pilu		2.23	0.50	0.11	50	235	0.745	39	21	18	65	163	17	142	-	5	-	-
Waisisi		1.24	0.66	0.124	140	610	0.870	58	23	12	40	207	26	148	-	7	-	-
Iaupolo	W. Pergusson	*	*	*	*	*	1.18	18	27	4	159	91	21	485	-	11	-	-
Igwageta		*	*	*	*	*	1.18	28	34	11	159	93	12	333	-	9	-	-
Gaua	New Hebrides	3.84	0.88	0.263	73	1080	2.67	77	29	11	135	242	15	240	-	10	-	-
Vanualava		2.36	0.50	0.114	-	795	2.26	73	31	16	116	98	37	355	-	12	-	-
Lou Island	Admiralty	2.34	0.67	0.168	73	450	1.73	58	28	7	163	77	32	421	28	10	-	-
Pam		*	*	*	*	*	1.59	22	29	6	190	48	33	308	27	4	-	-
Lakou		*	*	*	*	*	2.45	58	37	4	153	92	31	514	38	3	-	-
Umrei		*	*	*	*	*	2.00	17	32	7	173	78	102	482	32	-	-	-
Te Mamavai	Easter Island	*	*	*	*	*	2.07	62	60	13	92	21	146	832	72	6	-	-
Maunga Orito		2.40	0.35	0.103	37	530	2.14	55	60	7	89	16	149	886	75	6	-	-
Hala'uta	Tonga	0.40	2.24	2.17	-	930	5.86	20	11	2	18	235	-	9	-	-	-	-
Tefito		0.81	1.88	1.35	-	750	2.86	24	13	9	29	259	7	43	-	-	-	-
Weta	New Zealand	4.24	0.44	0.042	-	145	0.86	65	44	62	563	-	84	111	24	32	-	-
Cook's Bay		*	*	*	*	*	1.14	33	24	5	153	82	26	142	-	12	-	-
Pitcairn	Hawaii	3.06	0.98	0.302	-	1270	4.14	58	59	11	88	54	55	800	69	5	-	-
Kermadecs		0.49	3.44	0.306	-	1150	3.73	31	23	10	11	186	24	56	-	2	-	-
Puu Waawaa		2.59	0.35	0.135	-	1750	2.17	42	32	6	104	12	34	778	-	6	-	-
Dobu	E. Pergusson	*	*	*	*	*	2.58	27	44	16	141	-	94	1185	-	15	-	-

* No measurement - Not detected

TABLE 6

INTERELEMENT CONCENTRATION RATIOS USING

THE PIXE TECHNIQUE

	K/Ca	Fe/Ti	Si/K*	Fe/Rb	Fe/Zr	Sr/Rb	Sr/Zr	Rb/Zr	Y/Zr	Nb/Zr
Al2	0.178	3.05	0.73	1810	16.1	4.35	0.039	0.009	0.45	1.66
A9	0.123	2.80	0.61	3590	20.2	14.1	0.079	0.006	0.43	1.66
A8	0.399	2.00	0.91	1120	13.3	5.23	0.062	0.006	0.32	2.08
Tikopia	0.189	14.7	0.87	792	169	3.31	0.705	0.21	0.11	0.075
Dire	3.58	6.3	0.47	136	56.0	3.77	1.55	0.41	0.13	
Mt Bao	3.55	6.6	0.49	140	54.5	3.74	1.45	0.39	0.070	
Talasea	3.57	6.6	0.52	151	66.7	3.74	1.65	0.44	0.080	
Hospital	3.39	6.5	0.50	168	66.5	4.19	1.66	0.40	0.16	
Bitokara	3.49	7.1	0.47	140	60.6	3.69	1.60	0.43	0.085	
Admin				136	55.7	3.85	1.58	0.41	0.11	
Garua	4.64	6.3	0.45	90.0	41.5	2.26	1.04	0.46	0.07	
Voganakai	4.23	6.7	0.45	132	58.3	2.67	1.18	0.44	0.09	
Pilu	4.46	6.8	0.45	115	52.5	2.51	1.15	0.46	0.12	
Waisisi	1.88	7.0	0.82	218	58.8	5.18	0.72	0.27	0.18	
Iaupolo				74.2	24.3	0.57	0.188	0.33	0.043	
Igwageta				74.2	35.4	0.59	0.279	0.48	0.036	
Gaua	4.36	10.2	0.25	198	111	1.79	1.01	0.56	0.063	
Vanualava	4.72	19.8	0.30	195	63.7	0.85	0.276	0.33	0.10	
Lou Island	3.49	10.3	0.43	106	41.1	0.47	0.183	0.39	0.076	
Pam				83.7	51.6	0.25	0.156	0.62	0.107	0.067
Lakou				160	47.7	0.60	0.179	0.30	0.060	0.088
Umrei				116	41.5	0.45	0.162	0.36	0.212	0.074
Te Mamavai				225	24.9	0.23	0.025	0.111	0.175	0.066
Maunga Orito	6.86	20.8	0.47	240	24.2	0.18	0.018	0.100	0.168	0.087
Hala'uta	0.179	2.70	1.46	3260	6510	13.1	26.1	2.0	0	0.085
Tefito	0.431	2.11	1.23	986	665	8.93	6.02	0.67	0.16	
Weta	9.63	20.5	0.45	15.3	77.4	0	0	5.1	0.76	0.216
Cook's Bay				74.5	80.3	0.54	0.577	1.08	0.18	
Pitcairn	3.12	13.7	0.28	470	51.8	0.61	0.068	0.110	0.069	0.086
Kermadecs	0.142	12.2	2.51	3390	666	16.9	3.32	0.20	0.43	
Hawaii	7.40	16.1	0.30	208	27.9	0.115	0.015	0.13	0.044	
Dobu				183	21.8	0	0	0.12	0.079	

* *The Si/K ratio is obtained from peak areas not from element concentrations.*

very clear indicators for this source region. Some of the interelement concentration ratios are shown in Figures 10, 11, 12 and 13. Figure 10 shows K/Ca concentrations plotted against Fe/Ti concentrations, Figures 11 and 12, Fe/Rb versus Fe/Zr and Figure 13, Sr/Zr versus Rb/Zr. The wide range of these interelement ratios and the separation of the samples are clearly seen. There is however, a grouping of the sources from the New Britain region and the Dire, Mt Bao, Admin, Bitokara and Talasea samples are not necessarily separable.

Calculation of correlation coefficients, using either the element concentrations or the interelement ratios with a weighting proportional to the original counts, provided a simple method for grouping the samples into source regions.

However, it was shown that intercomparison of samples using uncorrected counts into a number of windows (17), which were set up about the most prominent peaks in the X-ray spectra, was almost as satisfactory for source correlation as interelement concentration analysis. The data in low energy windows, where there is a high background contribution, are, however, much less sensitive to variation in elemental concentrations of minor elements.

7. CONCLUSION

The PIXE technique is a completely satisfactory method for the element analysis of obsidian glass requiring only a minimum of sample preparation. The method is therefore, being used in conjunction with a (p,γ) measurement to provide element concentrations in a complete survey of obsidian sources from the South West Pacific region. In this report, the range of element concentrations analysed in a sample included K, Ca, Ti, V, Mn, Fe, Ni, Ga, As, Rb, Sr, Y, Zr, Nb, Ta and Pb, but the installation of a newer detector has extended the range of elements to be analysed so that Na, Mg, Al and Si concentrations can also be measured.

8. ACKNOWLEDGEMENTS

We wish to thank W.R. Ambrose and B.F. Leach for providing us with the obsidian source samples used in the experiment. Thanks are due to H. Broe, J.P. Fallon and M.J. Kenny of the 3 MeV Van de Graaff accelerator operations staff. L.H. Russell and M.D. Scott installed the target chamber and its ancillary equipment and M.D. Scott and R.J. Cawley assembled and programmed the software for data acquisition.

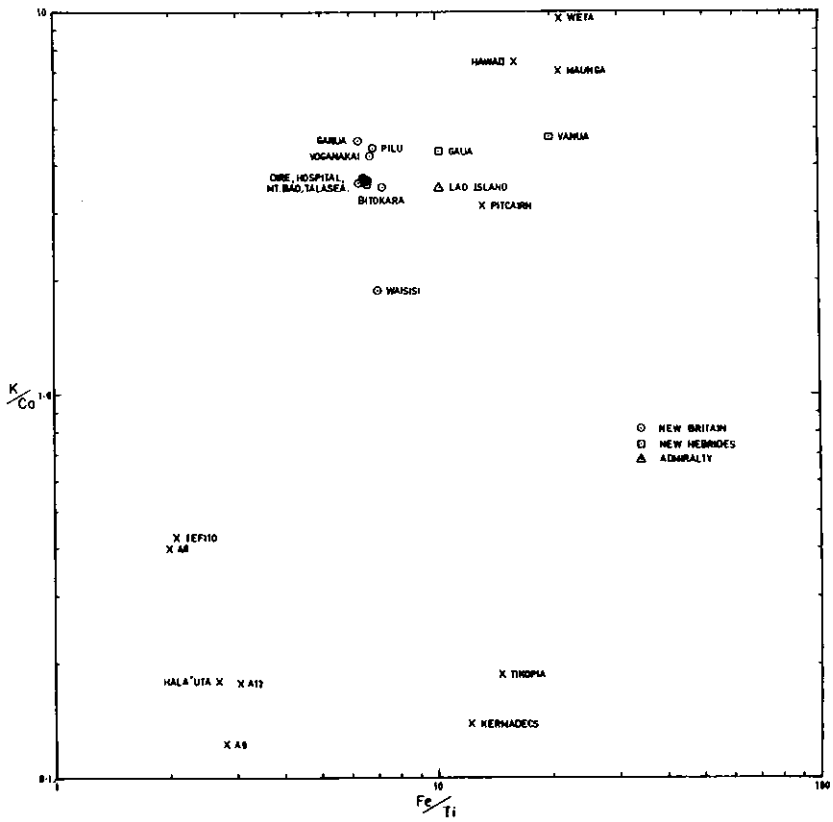

FIGURE 10. CONCENTRATION RATIOS K/Ca VERSUS Fe/Ti

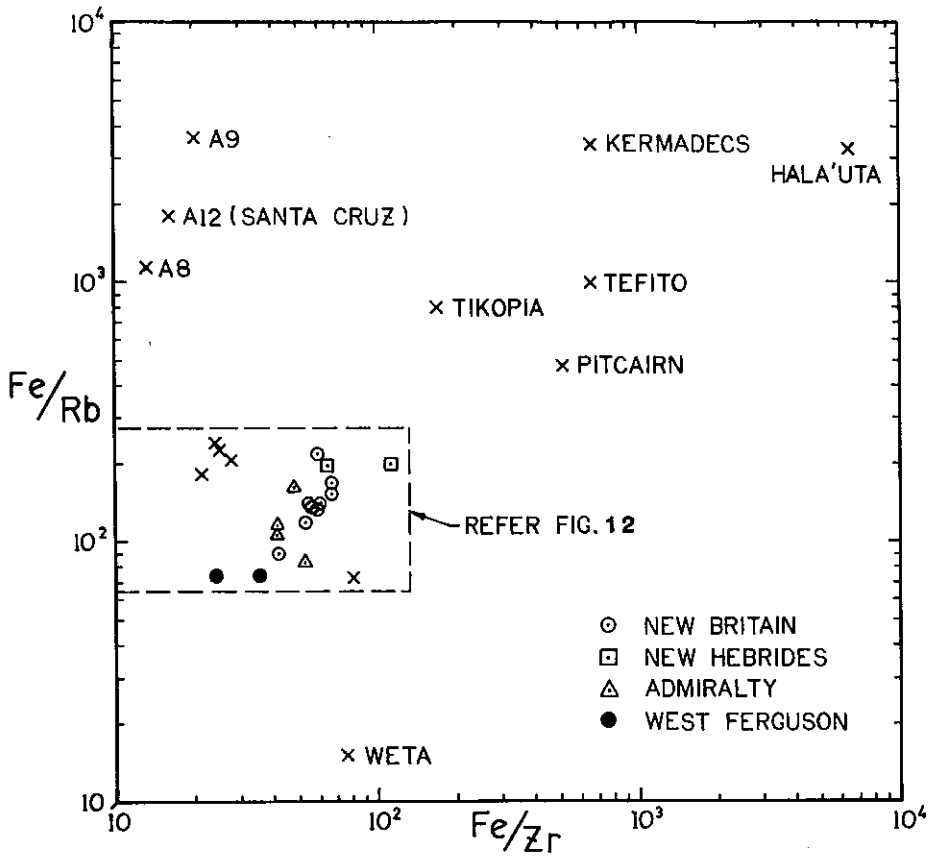

FIGURE 11. CONCENTRATION RATIOS Fe/Rb VERSUS Fe/Zr

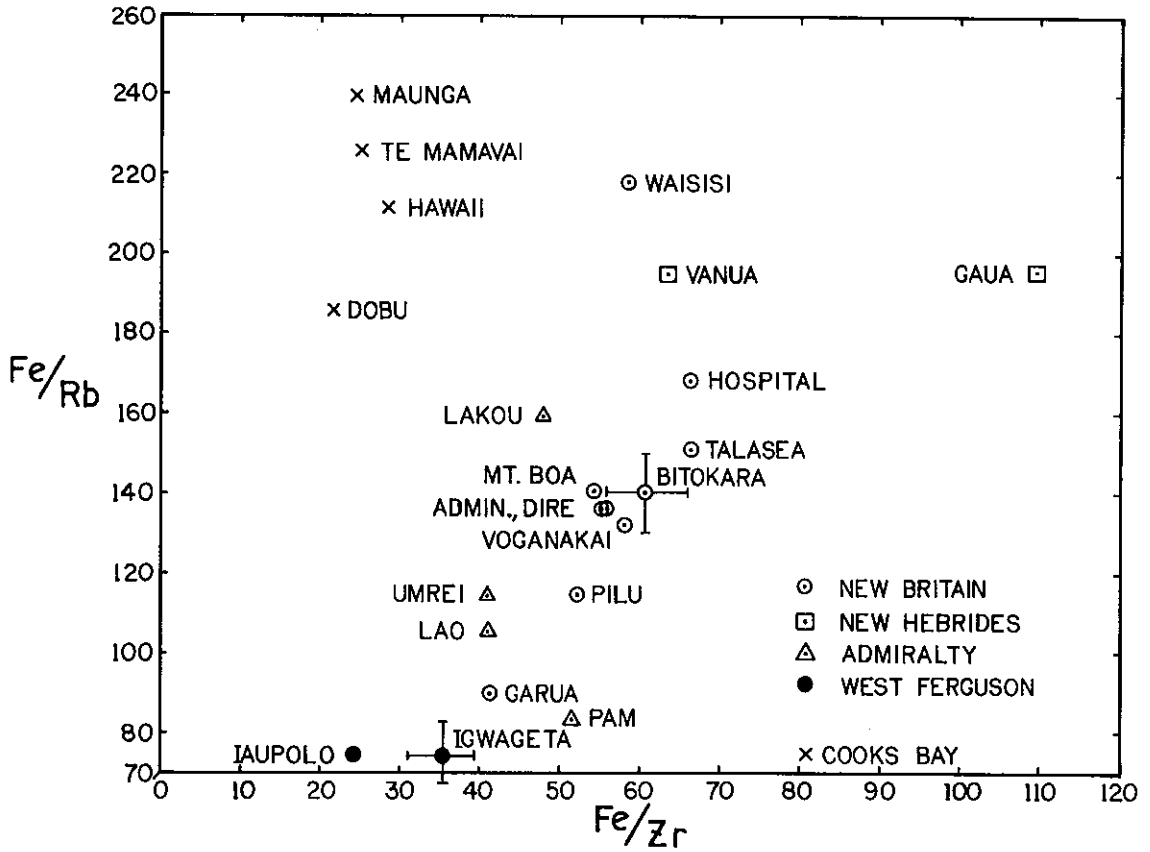

FIGURE 12. CONCENTRATION RATIOS Fe/Rb VERSUS Fe/Zr

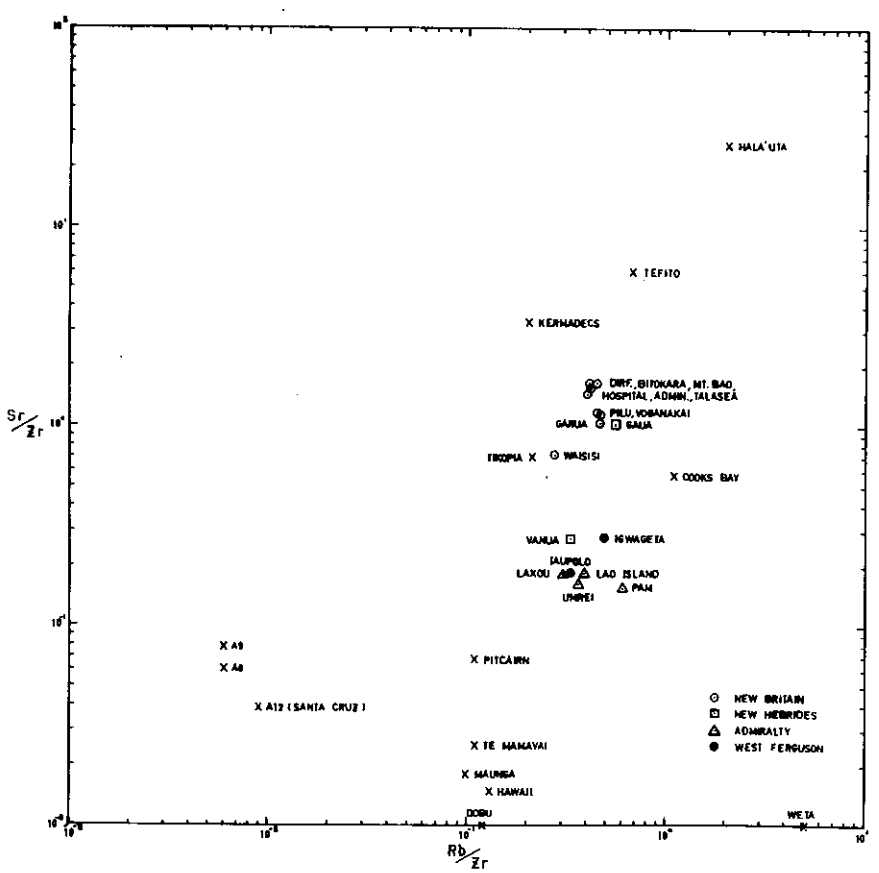

FIGURE 13. CONCENTRATION RATIOS Sr/Zr VERSUS Rb/Zr

9. REFERENCES

Ambrose, W.R. [1976] - private communication.

Bambynek, W., Crasemann, B., Fink, R.W., Freund, H.-U.. Mark, H., Swift, C.D., Price, R.E. & Venugopala, P. [1972] - *Rev. Mod. Phys.*, 44 : 716.

Bird, J.R., Russell, L.H., Scott, M.D. & Ambrose, W.R. [1978] - *Anal. Chem.*, 50 (14)2082-2084.

Cohen, D.D., Duerden, P. & Clayton, E. [1979] - AAEC/E468 (in press).

Cohen, D.D. & Duerden, P. [1979] - AAEC/E453.

Johansson, S.A.E. & Johansson, T.B. [1976] - *Nucl. Instrum. Methods*, 137 : 473-516.

Key, C.A. [1969] - *Arch. Phys. Anthrop. Oceania*, IV : 45-55.

Liebert, R.B., Zabel, T., Miljanic, D., Larsen, H., Volcovic, V. & Phillips, G.C. [1973] - *Phys. Rev.*, A8 : 236-241.

Neilson, K.K., Hill, M.W., Mangelson, N.F. & Nelson, F.W. [1976] - *Anal. Chem.*, 48 (13) 1947-1950.

Reed, S.J.B. [1965] - *Br. J. Appl. Phys.*, 16 (7) 913-926.

Reeves, R.D. & Ward, G.K. [1976] - Characterisation Studies of New Zealand Obsidian: Towards a Regional Prehistory. In *Advances in Obsidian Glass Studies - Archeological and Geochemical Perspectives* (ed. R.E. Taylor), Noyes Press, Park Ridge, N.J.

Reuter, W., Lurio, A., Cardone, F. & Ziegler, J.F. [1975] - *J. Appl. Phys.*, 46 (7) 3194-3202.

Rogers, G. [1974] - *J. Polynesian Soc.*, 83 (3)

Smith, I.E. [1974] - *Arch. Phys. Anthrop. Oceania*, IX : 18-25.

Smith, I.E.M., Ward, G.K. & Ambrose, W.R. [1977] - *Arch. Phys. Anthrop. Oceania*, XII : 173-201.

Theisen, R. & Vollath, D. [1967] - Tables of X-ray Mass Attenuation Coefficients, Verlag Stahleisen GMbH, Düsseldorf.

Williamson, C.F., Boujot, J. & Picard, J. [1966] - CEA-R3042.

Willis, R.D. & Walter, R.L. [1977] - *Nucl. Instrum. Methods*, 142 : 231-242.